nature physics

SUPPLEMENTARY INFORMATION

DOI: 10.1038/NPHYS3949

Fermi polaron-polaritons in charge-tunable atomically thin semiconductors

Meinrad Sidler, Patrick Back, Ovidiu Cotlet, Ajit Srivastava[†], Thomas Fink, Martin Kroner, Eugene Demler[*], and Atac Imamoğlu

Institute of Quantum Electronics, ETH Zürich, CH-8093 Zürich, Switzerland.

[†]*Physics Department, Emory University, Atlanta, Georgia 22138, USA and*

[*]*Physics Department, Harvard University, Cambridge, Massachusetts 02138, USA*

(Dated: September 27, 2016)

DOI: 10.1038/NPHYS3949

Although in the experiments we have a 0D cavity, these experiments can be extended to a system with a 2D cavity. Therefore, in the theory section we will analyse the latter case. The 0D cavity case will appear as a special case of our result. However, in considering a 2D cavity we show that ultra-low mass polarons can easily be obtained experimentally by exchanging the 0D cavity with the 2D cavity.

To analyse this problem it is useful to disentangle the different energy scales. By far the largest energy scale in our problem is set by the exciton binding energy E_{exc}, which, in the absence of electron doping, is estimated to be $\approx 0.5eV$. In TMDs, there are 16 different types of excitons that can be formed in the K and $-K$ valleys. Out of these, only 4 types of excitons are bright. Two of them have similar energies and are called A excitons, while the other two have significantly larger binding energies and are called B excitons. In the presence of a Fermi sea (ignoring the effect of exciton-electron interactions) the exciton binding energy will be reduced by $\delta(E_F)$ (of the order of E_F) due to phase-space filling, screening due to the 2DES, and band-gap renormalisation. An accurate calculation of $\delta(E_F)$ is beyond the scope of this paper and therefore, for simplicity, we take $\delta(E_F) \propto \beta e_F$, where β is a material dependent fitting parameter. We remark that the most of the polaronic features that we investigate in this paper are independent of the funciton $\delta(E_F)$.

After obtaining the full exciton spectrum, we can investigate the interactions between excitons and electrons. We focus on the lowest lying $1s$ exciton orbital assuming that the gap to the higher lying excitonic states, $E_{2s}-E_{1s}$, is much larger than the other energy scales in the problem. The exciton-electron interaction will have three contributions. The direct Coulomb interaction will be zero because the exciton is a neutral particle, and there is a near perfect symmetry between the electron and the hole forming the exciton, since the electron and the hole masses are similar. The second type of interaction is dipole-charge interaction which arises from the perturbative coupling of the $1s$ exciton to the higher lying exciton states. The third type of interaction is due to exchange of a Fermi sea electron with the electron of the exciton. This interaction, which can lead to the coupling between excitons in different valleys, is short ranged since the two electrons need to overlap, in order for exchange to be possible. In this work, we focus on the low n_e limit (i.e. $k_F a_B \ll 1$, where a_B is the exciton Bohr radius), where the most relevant interaction is the dipole-charge coupling. This allows us to ignore the other excitons and focus only on one of the $1s$ A excitons and ignore the other states. Furthermore, in the limit of small Fermi energies, we can treat the dipole-charge coupling as a contact interaction. Although we start from a general interaction, at a later point in the analysis we will use this contact interaction approximation because it greatly simplifies the analysis. However, in principle, the problem can be analysed without making the contact interaction approximation.

In light of the above arguments, it is justified to write down the following Hamiltonian describing a mobile bosonic impurity embedded in a fermionic reservoir:

$$H = \sum_k \omega_C(k) c_k^\dagger c_k + \sum_k \omega_X(k) x_k^\dagger x_k + \sum_k g(c_k^\dagger x_k + h.c.) + \sum_k \epsilon(k) e_k^\dagger e_k + \sum_{k,k',q} V_q x_{k+q}^\dagger e_{k'-q}^\dagger e_{k'} x_k \tag{1}$$

$$\omega_C(k) = \omega_c + \frac{\hbar k^2}{2m_c}, \quad \omega_X(k) = -E_{exc} + \frac{\hbar k^2}{2m_{exc}} + \delta(E_F), \quad \epsilon_k = \frac{\hbar k^2}{2m_e}, \tag{2}$$

where c, x and e are the destruction operators of a cavity photon, an exciton and an electron respectively, while m_c, m_x and m_e are the masses of the cavity photon, exciton and the electron. The third term corresponds to the coupling between excitons and the cavity field, while the last term incorporates the interaction between the exciton and the Fermi sea. Although we consider the exciton to be a rigid object, the interaction between the exciton and the Fermi sea contains the effects due to electron exchange between the exciton and the Fermi sea.

Chevy Ansatz for the polaron

In order to analyze the problem we make a Chevy-type Ansatz [1] for the polaron state, which truncates the Hilbert space to a single electron-hole pair:

$$|\Psi^{(p)}\rangle = \left(\phi_0 x_p^\dagger + \varphi_0 c_p^\dagger + \sum_{k,q} \phi_{k,q} x_{p+q-k}^\dagger e_k^\dagger e_q + \sum_{k,q} \varphi_{k,q} c_{p+q-k}^\dagger e_k^\dagger e_q \right) |0\rangle \tag{3}$$

where we defined the vacuum $|0\rangle$ as an undisturbed Fermi sea and no excitons in the system. In the following we will use the convention that $k, k' > k_F$ and $q, q' < k_F$. This ansatz takes into account the total momentum conservation

in our system and describes a quasi particle of momentum p formed by the superposition of a cavity photon and an exciton dressed by an electron-hole pair from the Fermi sea. To obtain the ground-state we must minimize the quantity $\langle\Psi^{(p)}|E-H|\Psi^{(p)}\rangle$:

$$\langle\Psi^{(p)}|E-H|\Psi^{(p)}\rangle = E\left(|\phi_0|^2+|\varphi_0|^2+\sum_{k,q}|\phi_{k,q}|^2+\sum_{k,q}|\varphi_{k,q}|^2\right)-H^{(p)}_{\rm var} \tag{4}$$

$$H^{(p)}_{\rm var}=\langle\Psi^{(p)}|H|\Psi^{(p)}\rangle=\omega_X(p)|\phi_0|^2+\omega_C(p)|\varphi_0|^2+\sum_{k,q}E_X(p,k,q)|\phi_{k,q}|^2+\sum_{k,q}E_C(p,k,q)|\varphi_{k,q}|^2 \tag{5}$$

$$-g\left[\phi_0^*\varphi_0+\sum_{k,q}\phi^*_{k,q}\varphi_{k,q}+c.c.\right]+|\phi_0|^2\sum_q V_0+\sum_{k,q}[\phi_0^*\phi_{k,q}V_{k-q}+c.c.] \tag{6}$$

$$+\sum_{k,q,k'}\left[\phi^*_{k,q}\phi_{k',q}V_{k-k'}+c.c.\right]-\sum_{k,q,q'}\left[\phi^*_{k,q}\phi_{k,q'}V_{q-q'}+c.c.\right] \tag{7}$$

where $E_X(p,k,q)\equiv\omega_X(p+q-k)+\epsilon(k)-\epsilon(q)$ and $E_C(p,k,q)\equiv\omega_C(p+q-k)+\epsilon(k)-\epsilon(q)$. Each term in H_{var} corresponds to a physical process allowing the observation of the competition between different processes, in trying to minimise H_{var} subject to the normalisation constraint. Minimizing the above equation, we obtain the following equations:

$$\omega_C(p)\varphi_0-g\phi_0=E\varphi_0 \tag{8}$$

$$E_C(p,k,q)\varphi_{k,q}-g\phi_{k,q}=E\varphi_{k,q} \tag{9}$$

$$\omega_X(p)\phi_0-g\varphi_0+\sum_q\phi_0V_0+\sum_{k,q}\phi_{k,q}V_{k-q}=E\phi_0 \tag{10}$$

$$E_X(p,k,q)\phi_{k,q}-g\varphi_{k,q}+V_{k-q}\phi_0+\sum_{k'}V_{k'-k}\phi_{k',q}-\sum_{q'}V_{q'-q}\phi_{k,q'}=E\phi_{k,q} \tag{11}$$

Because the cavity coupling does not mix different momentum states, we can eliminate the first two equations and obtain a set of two equations:

$$\left(\omega_X(p)-\frac{g^2}{\omega_C(p)}\right)\phi_0+\sum_q\phi_0V_0+\sum_{k,q}\phi_{k,q}V_{k-q}=E\phi_0 \tag{12}$$

$$\left(E_X(p,k,q)-\frac{g^2}{E_C(p,k,q)}\right)\phi_{k,q}+V_{k-q}\phi_0+\sum_{k'}V_{k'-k}\phi_{k',q}+\sum_{q'}V_{q'-q}\phi_{k,q'}=E\phi_{k,q} \tag{13}$$

Notice that the effect of the cavity is to renormalise the energies of many body states. The correction is recognised as the exact self-energy due to interactions with the cavity field.

At this point it is straightforward to solve the problem by discretizing the momenta k,q and transforming the above equations into a matrix equation.

However, we can make further analytical progress by making a few reasonable approximations. First of all, as mentioned before, the exciton-electron interaction is a Van der Waals interaction with a range given by the Bohr radius a_B of the excition. Including the screening effects due to the electron-system, the interaction will become even shorter range. Therefore, at least for small Fermi energies (i.e. $a_Bk_F\ll1$) we can approximate the interaction with a contact interaction which is constant $V_k=V$ up to a cutoff Ω. In two dimensions, an attractive potential always has a bound state. In our case we denote the energy of the bound state by $-E_T$ and we can express the interaction strength as a function of the bound state energy and an ultra-violet cutoff [2]:

$$\frac{1}{V}=-\sum_{k=0}^{\Omega}\frac{1}{E_T-\omega_X(0)+\omega_X(k)+\epsilon(k)} \tag{14}$$

Since the physics should not depend on the ultraviolet cutoff, in the end we will let $\Omega\to\infty$ and therefore $V\to0$. As we will show a posteriori, $\phi_{k,q}\sim1/k^2$ for large k, which in turn implies that the last term on the left hand side vanishes when $V\to0$. We will therefore proceed by neglecting this term.

DOI: 10.1038/NPHYS3949

We introduce the function $\chi_q = \phi_0 + \sum_k \phi_{k,q}$. In terms of this function:

$$\phi_0 = \frac{V\sum_q \chi_q}{E - \omega_X(p) + \frac{g^2}{\omega_C(p)}} \tag{15}$$

$$\phi_{k,q} = \frac{V\chi_q}{E - E_X(p,k,q) + \frac{g^2}{E_C(p,k,q)}} \tag{16}$$

Reintroducing the above into the definition of χ_q we can obtain the following self-consistent equation:

$$E = \omega_X(p) + \frac{g^2}{E - \omega_C(p)} + \sum_q \left[\sum_{k=0}^{\Omega} \frac{1}{E_T - \omega_X(0) + \omega_X(k) + \epsilon(k)} - \sum_{k=k_F}^{\Omega} \frac{1}{E - E_X(p,k,q) + \frac{g^2}{E - E_C(p,k,q)}}\right]^{-1} \tag{17}$$

To gain further insight into the above equation we introduce the polariton dispersion resulting from linearly coupling two harmonic oscillator modes of energies $E_X(p,k,q)$ and $E_C(p,k,q)$ with a coupling strength g_c:

$$\Omega_{LP,UP}(p,k,q) = \frac{1}{2}\left[E_X(p,k,q) + E_C(p,k,q) \pm \sqrt{\left(E_X(p,k,q) - E_C(p,k,q)\right)^2 + 4g_c^2}\right] \tag{18}$$

We also introduce the factors yielding the exciton fractions in polaritons. which show how much of the initial modes is contained in the new modes:

$$|X(p,k,q)|^2 = \frac{1}{2}\left(1 + \frac{E_C(p,k,q) - E_X(p,k,q)}{\sqrt{\left(E_C(p,k,q) - E_X(p,k,q)\right)^2 + 4g_c^2}}\right) \tag{19}$$

With the above notation we can rewrite the self consistent equation as:

$$E - \omega_X(p) = \frac{g^2}{E - \omega_C(p)} + \sum_q \left[\sum_{k=0}^{\Omega} \frac{1}{E_T - \omega_X(0) + \omega_X(k) + \epsilon(k)} - \sum_{k=k_F}^{\Omega} \left(\frac{|X(p,k,q)|^2}{E - \Omega_{LP}(p,k,q)} + \frac{1 - |X(p,k,q)|^2}{E - \Omega_{UP}(p,k,q)}\right)\right]^{-1} \tag{20}$$

We can simplify things further by noting that for $p + q - k > k_{ph}$ (k_{ph} is of the order of the photon momentum and approximately given by $\hbar k_{ph}^2/(2m_c) = g_c$) $X(p,k,q) \approx 1$ and $\Omega_{LP}(p,k,q) \approx E_X(p,k,q)$. Since k_{ph} is much smaller than all the other momentum scales the phase space where these approximations break down is extremely small. Based on this phase-space argument we can simplify the above equation:

$$E = \omega_X(p) + \frac{g^2}{E - \omega_C(p)} + \sum_q \left[\sum_{k=0}^{\Omega} \frac{1}{E_T - \omega_X(0) + \omega_X(k) + \epsilon(k)} - \sum_{k=k_F}^{\Omega} \frac{1}{E - E_X(p,k,q)}\right]^{-1} \tag{21}$$

We would have obtained the same equation if we had started from an Ansatz which did not contain the states corresponding to a photon dressed by an electron-hole pair (i.e. $\varphi_{k,q} = 0$). Our full derivation serves to justify this approximation. We remark that the poles in the q summation correspond to the molecular energies that are obtained when choosing an ansatz of the form $|\Phi^{(p)}\rangle = \phi_k x_{p-k}^\dagger e_k^\dagger e_p |0\rangle$.

It can be shown that by replacing $E \to E + i\eta$ ($\eta \to 0^+$), the last term on the right hand side of the above equation is the self-energy of an exciton interacting with a Fermi sea. Although the inclusion of the infinitesimal $i\eta$ might seem arbitrary at this point, it can be shown that it emerges from choosing a time dependent ansatz, where one minimises the action $S = \int \langle\Psi(t)|i\partial/\partial t - H|\Psi(t)\rangle$ instead of minimising $\langle\Psi|H|\Psi\rangle$ [3]. Therefore, the above equation can be written more intuitively as:

$$E = \omega_X(p) + \Sigma_X(E,p) \tag{22}$$

$$\Sigma_X(E,p) = \Sigma_{X-C}(E,p) + \Sigma_{X-e}(E,p) \tag{23}$$

$$\Sigma_{X-C}(E,p) = \frac{g^2}{E - \omega_C(p)} \tag{24}$$

$$\Sigma_{X-e}(E,p) = \sum_q \left[\sum_{k=0}^{\Omega} \frac{1}{E_T - \omega_X(0) + \omega_X(k) + \epsilon(k)} - \sum_{k=k_F}^{\Omega} \frac{1}{E + i\eta - E_X(p,k,q)}\right]^{-1} \tag{25}$$

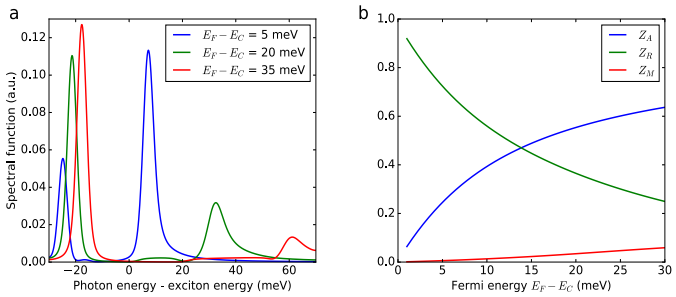

FIG. S1. Left panel we plot the spectral function $A(\omega)$ for different values of E_F. Right panel: the quasi-particle weight of the attractive polaron(blue), repulsive polaron (green) and the molecule+hole continuum (red) as a function of the Fermi energy

In the above we made explicit the self energy of the exciton interacting with the cavity mode (Σ_{X-C}) and with the electrons in the Fermi sea (Σ_{X-e}).

Having found the self-energy of the exciton, we can also obtain the self-energy of the cavity photon:

$$\Sigma_C(E,p) = \frac{g^2}{E - \omega_X(p) - \Sigma_{X-e}(E,p)} \tag{26}$$

.

Spectral Function

In the weak-coupling regime, in our experiment, we are probing the exciton spectral function:

$$A(t) = \langle 0|x_0 e^{-iHt} x_0^\dagger|0\rangle \tag{27}$$

In the truncated basis the Fourier transform of the spectral function is given by:

$$A(\omega) = \frac{1}{\pi}\mathrm{Im}\left[\frac{1}{\omega + i\eta - \omega_X(0) - \Sigma_X(\omega,0)}\right] \tag{28}$$

In the strong coupling regime we are probing the spectral function of the cavity photon and therefore, in the above we should replace Σ_X with Σ_C.

In simulating the experimental results we chose a lifetime broadening of $\eta = 1meV$ for both the bare exciton and the cavity-mode resonances. Since the exciton is also subject to disorder broadening, in the weak coupling regime we convolve the resulting spectral function with a Gaussian kernel with a standard deviation of $3meV$ (such that $FWHM = 6meV$).

We present the exciton spectral function obtained for $E_T = 25meV$, and three different Fermi energies in the left panel of Fig. S1. We choose $\beta = 0$, to illustrate the reasons for the identification of the resonances that appear as attractive/repulsive polarons.

We notice that one peak appears at the trion resonance $-E_T$ and redshifts (attractive polaron), while the other peak starts at the exciton energy and blue shifts with increasing Fermi energy (repulsive polaron). We also see a continuum of states of width $\approx 2/3E_F$ and very small oscillator strength which we identify as a trion+hole continuum. Due to its small oscillator strength, the continuum is better visible in logarithmic scale as presented in Fig. 4c of the main text.

The attractive polaron is a quasi-particle resulting from the mixing of an exciton with trion+hole pairs, and therefore our polaron ansatz includes these trion+hole states. Since the hole can be taken from anywhere inside the Fermi sea, we expect these states to form a continuum of width $\approx 2/3E_F$. We expect this continuum of states to start at the trion binding energy $-E_T$ at zero Fermi energy and to blue shift with the Fermi energy, due to phase-space filling, which modifies the trion binding energy. This blue-shift is in addition to the blue-shift of the exciton due to screening effects, phase space filling and band-gap renormalisation. Futhermore, the trion+hole states have vanishingly small oscillator strength: due to the momentum conservation, the emission of a photon due to exciton recombination must leave behind a Fermi sea electron-hole pair of zero momentum, a process which has a vanishingly small phase space. However, the hybridization of the trion+hole continuum with the exciton will yield a polaron with a large oscillator

DOI: 10.1038/NPHYS3949

strength while also resulting in slighly modified trion-hole states with a small but non-zero oscillator strength. Based on these features we can identify the continuum appearing above the attractive polaron state with the trion+hole continuum.

We notice that the quasiparticle weight is transferred from the repulsive to the attractive polaron. We illustrate this transfer in the right panel of Fig. S1. We again notice that the weight of the molecule+hole continuum remains negligible.

We remark that a complementary analysis of the different peaks can be performed by looking at the wavefunction corresponding to the states at different frequencies. To do this, we started from Eq. 12 and 13, made the contact interaction approximation, then discretized momentum space and turned the equations into a matrix eigenvalue equation, which we solved by explicit diagonalization. In this way we obtain a similar spectral function, but in addition we could also investigate the wavefunctions of of the states at each energy. This confirmed our interpretation of the spectral function.

Polaron mass

Having found the exciton self-energy we can also determine the effective mass of the exciton due to the interaction with the light cavity photon and the electron system. Assuming that the lowest energy state is at energy E_0 and momentum 0, the effective mass is given by:

$$\frac{1}{m^*} = \frac{1}{m_x} + \frac{\partial}{\partial^2 p}\Sigma_X(E_0,p)\bigg|_0 = \frac{1}{m_x} + \frac{1}{m_c} + \frac{\partial}{\partial^2 p}\Sigma_{X-e}(E_0,p)\bigg|_0 \tag{29}$$

Regardless of the contribution of the last term in the above equation we can see that, due to the small mass of the cavity photon, the polaron mass is going to be ultra-small. Therefore, we conclude that we are dealing with an ultra-low mass polaron. We emphasize that an ultra low mass polaron can only be achieved by dressing of a (polariton) impurity which is a superposition of an ultra-low mass particle (cavity photon) with a relatively heavy particle (exciton). Such a mixed-impurity exhibits an ultra-small mass for low momenta but restricts the recoil energy to the coupling energy g_c. Otherwise, if we did not have the relatively heavy particle, the dressing of an ultra-low mass impurity is very ineffective since $E_T \to 0$ for the same V. This means that the impurity will not be at all affected by the Fermi sea.

CAPACITIVE MODEL FOR THE FERMI ENERGY

By applying a top gate voltage V_g the electron density in the sample and therefore the Fermi energy E_F is changed. We denote the smallest V_g for which the attractive polaron is observed as $V_g = V_c$ which we interpret as the gate voltage for which we start populating the conduction band ($E_F > 0$).

The capacitance per unit area C/A between top gate and sample is given by:

$$\frac{C}{A} = \left(\frac{t}{\epsilon\epsilon_0} + \frac{1}{e^2 \mathrm{D}(E)}\right)^{-1}, \tag{30}$$

where $\mathrm{D}(E)$ is the density of states and $t \approx 105$ nm, $\epsilon \approx 3$ [4] are the thickness respectively the permittivity of the hBN flake. The two terms are the geometric respectively quantum capacitance of the sample. For $E_F > 0$, the quantum capacitance can be neglected since its effect is much smaller and within the uncertainty of the permittivity of the hBN flake. For $V_g > V_c$ i.e. $E_F > 0$ this yields:

$$E_F = \frac{\pi\hbar^2\epsilon\epsilon_0}{tem^*}(V_g - V_c) \approx 0.77\frac{\mathrm{meV}}{\mathrm{V}}(V_g - V_c), \tag{31}$$

where m^* is the effective electron mass of the conduction band.

We emphasize that the electron density dependent blue (red) shift of the absorption (photoluminescence) resonances strongly suggest that the injected electrons form a 2DES. In addition, the narrow exciton linewidth of ~ 5 meV and the small Stokes shift of ~ 2 meV between the absorption and photoluminescence peaks indicate that the role of localized excitonic states in our sample is minor.

SPATIAL DEPENDENCE

One of the principal advantages of the open fiber cavity structure is the ability to adjust the cavity length and to thereby change the nature of coupling. In our setup, the fiber facet and the substrate form a small angle. As a consequence, when the fiber is in close proximity to the facet it touches the substrate. The contact is located at the edge of the fiber which is 125 μm in diameter. This contact stabilizes the cavity by suppressing the vibrations that would otherwise have lead to line broadening. Furthermore, once the cavity is brought into contact with the substrate, changing the cavity length by changing the piezo voltage of the z-axis nanopositioner seems to be completely reversible. When the cavity length is reduced further to a few micrometers, it is essentially the fiber angle that changes and reduces the cavity length at the dimple which is in the center of the fiber facet.

Additionally, scanning the sample with respect to the fiber mirror allows us to investigate the spatial dependence of the $MoSe_2$ optical excitations. In order to investigate the latter, the cavity length was enlarged to be sure to eliminate any contact between fiber and substrate. At a cavity length of $\sim 30\mu$m, the sample was moved with respect to the fiber mirror with nanopositioner slip-stick steps. The nanopositioner resistive readout was used to get an estimate of the traveled distance. A rough estimate of the cavity positon with respect to the flake is obtained using a camera by imaging the flake illuminated with a green LED which is transmitted through a transmission window of the DBR. The spectrum is derived from the cavity linewidth broadening in a cavity length scan using the same technique as for the data shown in Figure 2 of the main text.

Figure S2 shows absorption spectra for different positions of the sample with respect to the cavity. The sample is moved by $\sim 0.5\,\mu$m in between the different measurements. The scan was measured at a gate voltage of $V_g = -10$ V where we expect to see absorption from both the repulsive and attractive polaron. At $x = -1.5\,\mu$m, the spatial overlap of the cavity mode with the $MoSe_2$ monolayer is small. As the sample is moved, the overlap and therefore the absorption increases until it reaches a maximum at $x = 0.0\,\mu$m. Moving the sample further up to $x = 1.5\,\mu$m reduces the overlap again. The absorption strength of the attractive polaron as compared to the repulsive polaron does not change significantly depending on the position of the sample which indicates a relatively homogeneous electron density. The large distance over which the absorption decreases is in accordance with the large cavity mode waist of 1.7 μm.

CAVITY MODE FITTING

The source for the transmission spectroscopy is a LED centered at $\sim$ 760 nm with a FWHM of $\sim$ 20 nm. For Figure 2a, Figure 3a,b,c and Figure 4a of the main text, the transmitted spectrum is normalized by the LED spectrum. For the derivation of the absorption spectrum of the flake from the transmission spectra shown in Figure 2a of the main text, the normalization with the LED spectrum is not necessary since only the linewidth and the center wavelength of the cavity mode but not the intensity of the transmitted cavity peaks are used to extract the absorption spectrum.

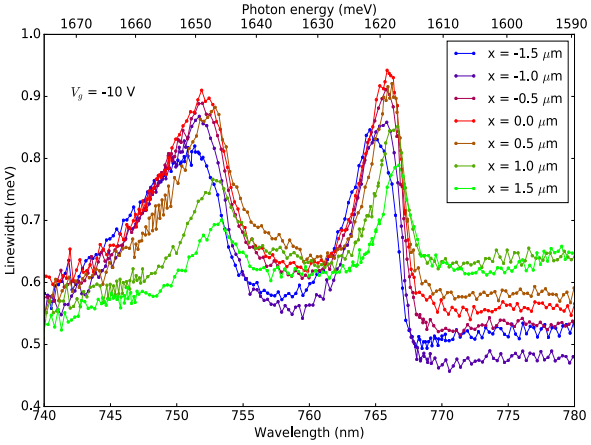

FIG. S2. Spatial dependence of the absorption spectrum.

DOI: 10.1038/NPHYS3949

In addition to the fundamental cavity mode, higher transverse modes are observed in the transmission spectrum. For fitting the lorentzian peak to the transmitted fundamental cavity mode, only the spectrum within a 4 nm wide window was considered in order to exclude distortions from the higher transverse modes.

At the cavity lengths used for weak coupling measurements, more than one fundamental (axial) mode are observed within the stop band of the DBR. For the derivation of the energy shift of the cavity due to the resonances of the flake, the cavity length is calculated from the wavelength of the next (lower-energy) fundamental mode. Since the energy of that cavity mode is smaller than any resonances of the $MoSe_2$ monolayer, its center wavelength serves as a good measure for the cavity length.

We note that for the cavity length of 9.1 μm used to obtain the data depicted in Fig. 2b, the exciton and the cavity are in the strong coupling regime for $V_g < -10$ V. As a consequence, it is not possible to obtain the imaginary part of the $MoSe_2$ linear susceptibility by measuring the excess cavity line broadening as we tune the cavity across the exciton (repulsive polaron) resonance. As a remedy, we chose to plot the linewidth of the cavity-like polariton peak for the parameter range corresponding to the dashed box in Fig. 2b. The cavity line broadening we extract in this manner is larger than the actual width of the exciton resonance. It does however, yield the correct exciton resonance frequency. As an alternative, it is possible to extract the actual imaginary part of the $MoSe_2$ linear susceptibility by fitting the data to a formula that describes the absorption lineshape in the presence of strong coupling [5] and extract an exciton linewidth of 4.5 meV. The drawback of the latter formula is that it is only accurate if the electronic resonances are Lorentzian; this is satisfied only for $V_g < -10$ V.

DIFFERENTIAL REFLECTION WITHOUT A CAVITY

As an independent confirmation of the measured electron density dependence of the absorption spectra, a second $MoSe_2$ monolayer was measured in differential reflection in the absence of a cavity. This monolayer is embedded in between hBN flakes and transfered onto a silicon substrate with a 285 nm thick SiO_2 layer. A gate voltage applied between the highly doped silicon substrate and the $MoSe_2$ monolayer flake enables us to change the electron sheet density in the sample. Given the higher capacitance between the gate and the flake, larger gate voltages are required to achieve similar electron densities as compared to the sample described in the main text. Using the capacitive model presented above, at the maximum applied gate voltage of 153 V, an electron sheet density of $n_e \approx 1.1 \cdot 10^{13}$ cm^{-2} is expected which corresponds to a Fermi energy of $E_F > 40$ meV (assuming a conduction band spin-orbit splitting of 30 meV). In accordance with the main text, it is assumed that the appearance of the blue shift of the repulsive polaron resonance marks the onset of filling the conduction band with electrons which in this sample is observed at a gate voltage of $V_g \sim -10$ V. We note that in both samples there is a V_g range ≥ 10 meV where the attractive polaron resonance is visible and yet neither of the two resonances exhibit a blue shift. We assume that in this V_g range the injected electrons are captured in localized states below the conduction band minimum and we have $E_F < E_C$.

The sample is measured in a cryostat at a temperature of 4 K. An LED is used as a broadband source and the reflection spectrum is measured at different electron densities. At a gate voltage of 153 V, the absorption of the sample is almost featureless due to large line broadening which is why the reflected spectrum at that backgate voltage is used for normalization. Since the peak absorption of the bare exciton resonance (in the absence of electrons) is stronger than the absorption of the attractive polaron, the measured spectra are plotted with two different color maps (Fig. S3a/b). The data is in excellent agreement with the absorption spectra measured with the cavity.

Figure S4 shows the energy of the attractive and repulsive polarons as a function of Fermi energy for both the sample embedded inside the fiber cavity and the second sample measured in differential reflection in the absence of a cavity. Possibly due to different dielectric environment, both attractive and repulsive polaron resonance in the latter sample were blue shifted by ~ 5 meV. Nevertheless, the observed energy shifts as a function of Fermi energy are in excellent agreement for the two samples (Fig. S4a). Figure S4b shows the difference between the attractive and repulsive polaron. Even though the uncertainty in the repulsive polaron energy is relatively large, especially for large Fermi energies, the agreement between the two samples is convincing. The peak position is determined by the position of the maximum absorption after smoothening the data with a Gaussian filter of 2 meV. The large uncertainty in the energy of the repulsive polaron is due to its increased linewidth and decreased absorption strength at large Fermi energies.

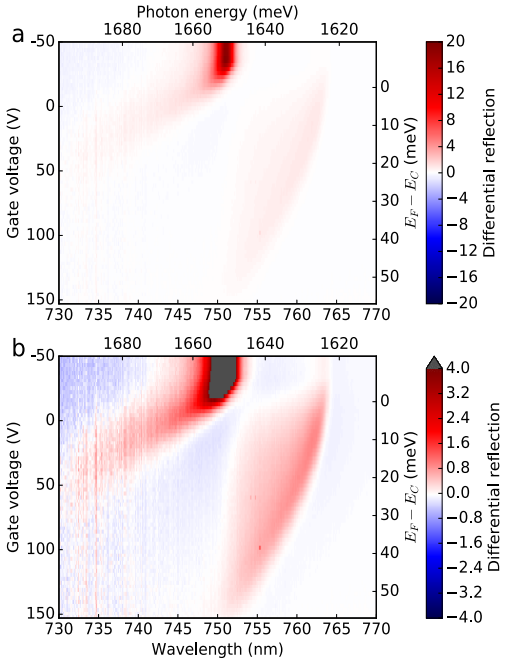

FIG. S3. **a** Electron density dependent differential reflection. **b** In a second color map, the large differential reflection of the repulsive polaron is clipped in order to increase the visibility of the attractive polaron resonance.

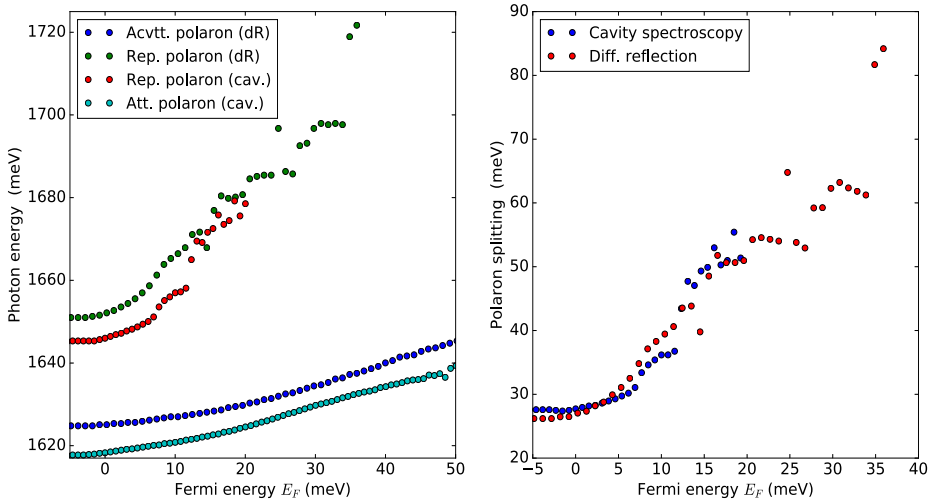

FIG. S4. **a** Energy of the attractive and repulsive polaron resonance as a function of Fermi energy for the sample embedded inside the fiber cavity (red, bright blue) and the second sample measured in differential reflection in the absence of a cavity. **b** Energy difference between attractive and repulsive polaron resonance as a function of energy for the two different samples (blue: embedded inside the fiber cavity, red: second sample in absence of the cavity).

DOI: 10.1038/NPHYS3949

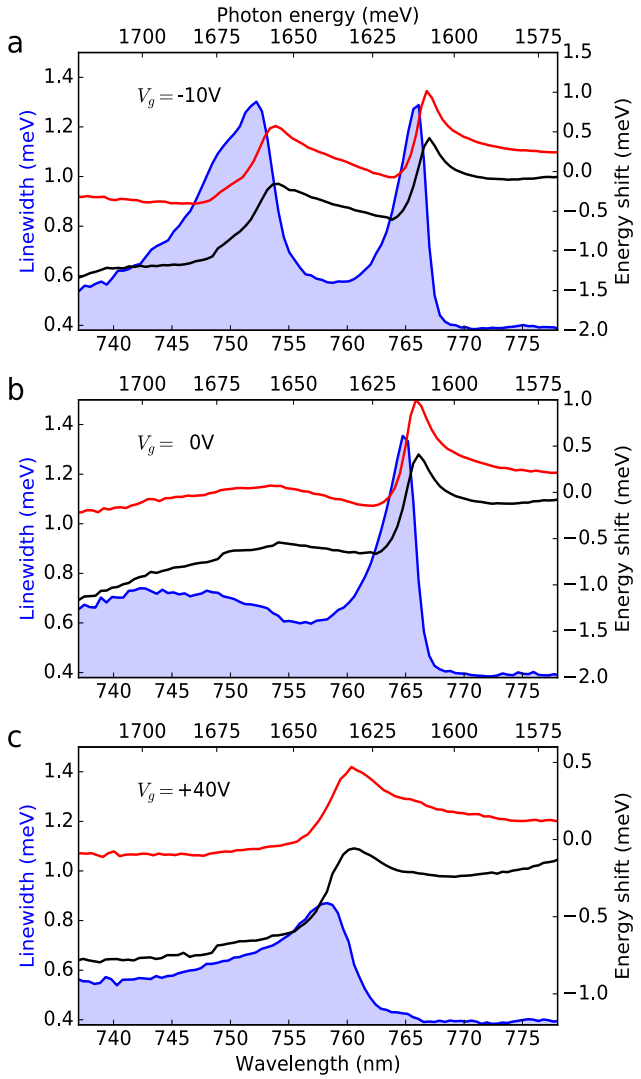

FIG. S5. Measured absorption (blue) and measured disperion (black) as well as the dispersion calculated from the absorption via Kramers-Kronig relations (red) for three different electron densities.

KRAMERS-KRONIG RELATION BETWEEN THE CAVITY-LINE BROADENING AND THE LINE-SHIFT

The microcavity experimental setup allows for measuring both the real and imaginary part of the susceptibility independently. Given the absorption spectrum, Kramers-Kronig relations allow for calculation of the dispersion. Figure S5 shows horizontal line cuts of the data in Fig. 2, depicting the absorption (blue) as measured through the linewidth of the cavity mode and the dispersion (black) as the energy shift of the cavity mode. The red curve is the expected dispersion as calculated from the measured absorption using Kramers-Kronig relations. The vertical displacement of the measured dispersion and the calculated dispersion is most likely a result of the simplified model of a cavity with an effective length given by the distance between the mirrors plus a wavelength independent penetration depth into the DBR. Correcting for the wavelength dependence of the penetration depth should get rid of this offset.

[1] F. Chevy, Physical Review A **74**, 063628 (2006).

[2] M. Randeria, J.-M. Duan, and L.-Y. Shieh, Physical review letters **62**, 981 (1989).
[3] M. M. Parish and J. Levinsen, Physical Review A **87**, 033616 (2013).
[4] K. K. Kim, A. Hsu, X. Jia, S. M. Kim, Y. Shi, M. Dresselhaus, T. Palacios, and J. Kong, ACS Nano **6**, 8583 (2012).
[5] S. E. Harris, J. E. Field, and A. Imamoğlu, Phys. Rev. Lett. **64**, 1107 (1990).